Journal of Solid Mechanics Vol. 11, No. 2 (2019) pp. 440-453
DOI: 10.22034/JSM.2019.665264

Influence of Viscoelastic Foundation on Dynamic Behaviour of the Double Walled Cylindrical Inhomogeneous Micro Shell Using MCST and with the Aid of GDQM

A. Mohammadi [1], H. Lashini [2], M. Habibi [3], H. Safarpour [4,*]

[1]*Faculty of Engineering, Department of Mechanics, Islamic Azad University of South Tehran Branch, Tehran, Iran*
[2]*Faculty of Mechanic and Manufacturing, University Putra Malaysia, Serdang, Malaysia*
[3]*Center of Excellence in Design, Robotics and Automation, School of Mechanical Engineering, Sharif University of Technology, Tehran, Iran*
[4]*Faculty of Engineering, Department of Mechanics, Imam Khomeini International University, Qazvin, Iran*

Received 22 March 2019; accepted 18 May 2019

ABSTRACT

In this article, dynamic modeling of double walled cylindrical functionally graded (FG) microshell is studied. Size effect of double walled cylindrical FG microshell are investigated using modified couple stress theory (MCST). Each layer of microshell is embedded in a viscoelastic medium. For the first time, in the present study, has been considered, FG length scale parameter in double walled cylindrical FG microshells, which this parameter changes along the thickness direction. Taking into consideration the first-order shear deformation theory (FSDT), double walled cylindrical FG microshell is modeled and its equations of motions are derived using Hamilton's principle. The novelty of this study is considering the effects of double layers and MCST, in addition to considering the various boundary conditions of double walled cylindrical FG microshell. Generalized differential quadrature method (GDQM) is used to discretize the model and to approximate the equation of motions and boundary conditions. Also, for confirmation, the result of current model is validated with the results obtained from molecular dynamics (MD) simulation. Considering length scale parameter ($l=R/3$) on MCST show, the results have better agreement with MD simulation. The results show that, length, thickness, FG power index, Winkler and Pasternak coefficients and shear correction factor have important role on the natural frequency of double walled cylindrical FG microshell.

Keywords : Double walled; Functionally graded material; Modified couple stress theory; Vibration analysis; Viscoelastic foundation.

1 INTRODUCTION

FG materials are a new group of materials which have many advantages and superior properties, including high temperature resistance and high strength. The applications of FG cylindrical shells can be very broad. The FG

*Corresponding author. Tel.: +98 9193771203.
E-mail address: hamed_safarpor@yahoo.com (H. Safarpour).

cylindrical shells can be applied to fuselage structures of civil airliners, aerospace structures, military aircraft propulsion system, and other engineering fields. In addition, the investigation of their vibration characteristics of FG cylindrical shell is of great interest for engineering design and manufacture. It is apparent from the literature survey that most research on FGMs has been restricted to vibration, fracture mechanics and optimization. Some researchers [1-8] investigated the vibration of cylindrical FG shells and panels. Also, FG material has a lot of application within micro/nano scale structures, for example : atomic force microscopes [9] and micro/nano electromechanical systems [10-13]. Here in, it must be prominent that when the sizes of structures change to the nano/micro scale, new phenomena are Appeared or constructed. The first one of these phenomena, when transforming macro to micro/nano scales, behavior of material properties depends on size effects. Some researchers studied that, modeling cylindrical nano or micro shells have been widely used in nano-scale devices and systems. As an example of application of micro shells, Mescher et al. [14] presented the buckling behaviors of microtubules in a living cell. It should be noted that the effect of scale is not included in the classical continuum theories, so this theory is not suitable for micro and nano scales. One of the non-classical theories that including the effect of scale is couple stress theory. Toupin, Koiter, and Mindlin [15-17] studied the couple stress theory containing higher order rotation gradients, which the asymmetric part of the deformation gradient. According to this theory, it has four material constants (two classical and two additional) for isotropic materials. For example of this theory, asghari et al. [18] investigated the effects of size scale in Timoshenko beams on the basis of the couple stress theory. Determination of the microstructure related length scale parameters are so difficult. In addition, we need to have a continuum theory which involves only one additional material parameter of length scale. One of the best and most convenient-known continuum mechanics theories that considered scale effects with reasonable accuracy in microscale devices is MCST. Yang et al [18] reported a modified couple stress theory, which the couple stress tensor is symmetric and just has a material length scale parameter is involved, different from the classical couple stress theory mentioned above. Some investigators have studied this theory to test the dynamic and static behavior of micro beams and plates [19-21]. It is noted that , nonlocal theory of Eringen is one of the best and most well-known continuum mechanics theories that includes small scale effects with good accuracy in nano/micro scale devices, but the results show that MCST coincides with experimental results better than Eringen's nonlocal elasticity and classical theories [22]. Therefore, in this study, the MCST has been used. Unique mechanical properties and extreme electrical conductivity of double-cylindrical shell structures have caused them to be of extensive use in various micro/nano devices. It is worth to maintaining that, dynamic behavior of double walled carbon tubes (DWCNTs) are similar to double cylindrical shell structures. Considering the use of DWCNTs in conveying fluids in Nano devices and the importance of identification of fluid-conveying DWCNTs, today many researchers attempt to scrutinize the dynamic behavior of these nanostructures [23-28]. In the field of stability of the cylindrical shell under various loading, Arani et al [29] presented buckling of a cylindrical shell in the neutron radiation environment, subjected to combined static and periodic axial forces. They in this work examine, influence of various parameters on stability of the cylindrical shell under different forces. In another works, electro-thermo-mechanical nonlinear dynamic buckling of an orthotropic piezoelectric nanocomposite cylindrical shell conveying viscous fluid is presented by Arani et al [30]. The important result is that, the dimensionless critical dynamic buckling load and stability of the structure increase when piezoelectric effect is considered.

In recently, zhang et al [25] are studied free and forced vibration analysis of circular cylindrical double-shell structures under arbitrary boundary conditions. The natural frequencies and mode shapes of the structures as well as frequency responses under forced vibration of their work are obtained with the Rayleigh–Ritz procedure. The novelty of this work is consideration of the size effect in the dynamic behavior of double moderately thick cylindrical FG microshell. The main idea of the present work is to propose a numerical model to study the free linear vibration of double FG micro shell using MCST, then applying the GDQM to solve it. The outer and inner cylindrical FG microshell material of this work is FG material and according to the power law distribution, it is assumed that the outer surface is metal and the inner surface is ceramic. The governing equations and boundary conditions have been developed using Hamilton principle. The results show that, length, thickness, FG power index, Winkler and Pasternak coefficient and shear correction factor play important roles on the natural frequency of the double walled cylindrical FG microshell.

2 GOVERNING EQUATIONS OF MOTION AND CORRESPONDING BOUNDARY CONDITIONS

Fig. 1 presents a schematic of the double walled cylindrical microshell. Moreover, this figure demonstrates the effect of the viscoelastic foundation between the two walls and the surroundings of this structure. L, R and h denote the

length, radius and the thickness of the double walled cylindrical microshell respectively. In this study, the double walled cylindrical microshell is modeled as two cylindrical viscoelastic shell.

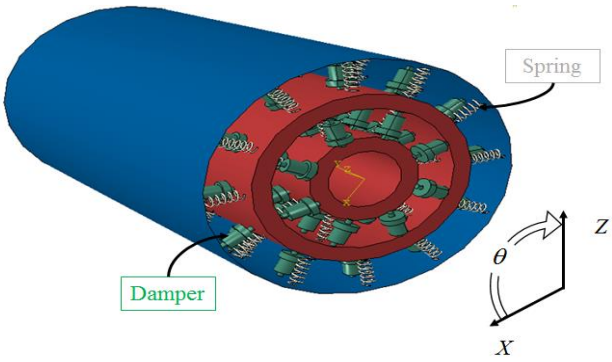

Fig.1
Geometry of a double walled cylindrical microshell.

According to the FSDT, the displacement field of each cylindrical shell along the three directions of x, θ, z would be as follows:

$$\begin{aligned} U(x,\theta,z,t) &= u(x,\theta,t) + z\psi_x(x,\theta,t) \\ V(x,\theta,z,t) &= v(x,\theta,t) + z\psi_\theta(x,\theta,t) \\ W(x,\theta,z,t) &= w(x,\theta,t) \end{aligned} \tag{1}$$

where, $u(x,\theta,t)$, $v(x,\theta,t)$, and $w(x,\theta,t)$ represent the displacements in axial, circumferential, and radial-directions respectively. $\psi_\theta(x,\theta,t)$ and $\psi_x(x,\theta,t)$ are the rotations about the circumferential and axial directions. In addition, strain tensor is expressed as:

$$\begin{aligned} \varepsilon_{ij} &= \frac{1}{2}(\Lambda_{i,j} + \Lambda_{j,i}), \\ \chi^s_{ij} &= \frac{1}{2}(\varphi_{i,j} + \varphi_{j,i}), \\ m^s_{ij} &= 2l^2\mu(\hat{z})\chi^s_{ij}. \end{aligned} \tag{2}$$

In Eq. (2) Λ_i and ϕ_i represent the components of displacement vector and infinitesimal rotation vector respectively. Furthermore, l is the parameter which denotes the additional and independent material length-scale parameter which has relates with the symmetric rotation gradients. At the inner and the outer surfaces, the FG nanoshell is generally composed of two different materials. The FG cylindrical nanoshell is made of porous material and according to the power law distribution, its bulk elastic modulus $E(z)$, mass density $\rho(z)$, and Poisson's ratio $v(z)$ are assumed to change along the thickness direction [31]. Power FG index (F) determines the variation profile of material properties across the cylindrical FG nanoshell thickness. Assuming that the inner surface is ceramic and the outer surface is metal, then for different values of F, the mechanical properties can be written as:

$$\begin{aligned} E(z) &= (E_m - E_c)(\frac{z}{h} + 0.5)^F + E_c \\ \rho(z) &= (\rho_m - \rho_c)(\frac{\hat{z}}{h} + 0.5)^F + \rho_c \\ \nu(z) &= (\nu_m - \nu_c)(\frac{\hat{z}}{h} + 0.5)^F + \nu_c \end{aligned} \tag{3}$$

The stress-strain equations in plane stress cases are written as follows for the elastic inhomogeneous moderately thick cylindrical microshell model:

$$\begin{Bmatrix}\sigma_{xx}\\ \sigma_{\theta\theta}\\ \sigma_{x\theta}\\ \sigma_{\theta z}\\ \sigma_{xz}\end{Bmatrix}=\begin{bmatrix}\frac{E(z)}{1-\nu^2(z)} & \frac{E(z)\nu(z)}{1-\nu^2(z)} & 0 & 0 & 0\\ \frac{E(z)\nu(z)}{1-\nu^2(z)} & \frac{E(z)}{1-\nu^2(z)} & 0 & 0 & 0\\ 0 & 0 & \frac{E(z)}{2(1+\nu(z))} & 0 & 0\\ 0 & 0 & 0 & \frac{E(z)}{2(1+\nu(z))} & 0\\ 0 & 0 & 0 & 0 & \frac{E(z)}{2(1+\nu(z))}\end{bmatrix}\begin{Bmatrix}\varepsilon_{xx}\\ \varepsilon_{\theta\theta}\\ 2\varepsilon_{x\theta}\\ 2\varepsilon_{\theta z}\\ 2\varepsilon_{xz}\end{Bmatrix} \tag{4}$$

The principle of minimum potential energy is used in order to derive the equations of motion and the associated boundary conditions:

$$\int_{t_1}^{t_2}(\delta T-\delta U+\delta W-\dot{\delta}D)dt=0 \tag{5}$$

where, U and T are strain and kinetic energies respectively. The strain energy of a cylindrical shell includes classical strain energy U_1, and non-classical strain U_2. Therefore, the variation of strain energy would be written as follows:

$$\delta U=\delta U_1+\delta U_2 \tag{6}$$

where,

$$\delta U_1=\frac{1}{2}\iiint_V(\sigma_{ij}\delta\varepsilon_{ij})dV=\iint_A\begin{Bmatrix}(N_{xx}\frac{\partial}{\partial x}\delta u+M_{xx}\frac{\partial}{\partial x}\delta\psi_x)+N_{\theta\theta}(\frac{1}{R}\frac{\partial}{\partial\theta}\delta v+\frac{\delta w}{R})+\\ M_{\theta\theta}\frac{1}{R}\frac{\partial}{\partial\theta}\delta\psi_\theta+Q_{xz}(\delta\psi_x+\frac{\partial}{\partial x}\delta w)+\\ N_{x\theta}(\frac{1}{R}\frac{\partial}{\partial\theta}\delta u+\frac{\partial}{\partial x}\delta v)+M_{x\theta}(\frac{1}{R}\frac{\partial}{\partial\theta}\delta\psi_x+\frac{\partial}{\partial x}\delta\psi_\theta)\\ +Q_{z\theta}(\delta\psi_\theta+\frac{1}{R}\frac{\partial}{\partial\theta}\delta w-\frac{\delta v}{R})\end{Bmatrix}Rdxd\theta$$

$$\delta U_2=\frac{1}{2}\iiint_V(m_{ij}^s\delta\chi_{ij}^s)dV=\iint_A\begin{Bmatrix}(-\frac{Y_{\theta\theta}}{2R^2}+\frac{Y_{zz}}{2R^2})\frac{\partial}{\partial\theta}\delta u-(\frac{Y_{\theta z}}{2R^2})\frac{\partial^2}{\partial\theta^2}\delta u-(\frac{Y_{zx}}{2R})\frac{\partial^2}{\partial\theta\partial x}\delta u\\ +(\frac{Y_{\theta\theta}}{2R}-\frac{Y_{xx}}{2R})\frac{\partial}{\partial x}\delta v+(\frac{Y_{xz}}{2})\frac{\partial^2}{\partial x^2}\delta v-(\frac{Y_{\theta x}}{2R^2})\frac{\partial}{\partial\theta}\delta v\\ +(\frac{Y_{\theta z}}{2R})\frac{\partial^2}{\partial\theta\partial x}\delta v+(\frac{Y_{xz}}{2R^2})\delta v+(\frac{Y_{\theta z}}{2R})\frac{\partial}{\partial x}\delta w-(\frac{Y_{\theta x}}{2})\frac{\partial^2}{\partial x^2}\delta w\\ -(\frac{Y_{zx}}{2R^2})\frac{\partial}{\partial\theta}\delta w+(\frac{Y_{x\theta}}{2R^2})\frac{\partial^2}{\partial\theta^2}\delta w+(-\frac{Y_{\theta\theta}}{2R}+\frac{Y_{xx}}{2R})\frac{\partial^2}{\partial\theta\partial x}\delta w\\ +(\frac{Y_{x\theta}}{2})\frac{\partial}{\partial x}\delta\psi_x+(\frac{Y_{\theta\theta}}{2R}-\frac{Y_{xx}}{2R})\frac{\partial}{\partial\theta}\delta\psi_x-(\frac{T_{zx}}{2R})\frac{\partial^2}{\partial\theta\partial x}\delta\psi_x\\ -(\frac{Y_{z\theta}}{2R})\delta\psi_x-(\frac{Y_{x\theta}}{2R})\frac{\partial}{\partial\theta}\delta\psi_\theta+(\frac{Y_{\theta\theta}}{2R}-\frac{Y_{xx}}{2}+\frac{Y_{zz}}{2})\frac{\partial}{\partial x}\delta\psi_\theta\\ +(\frac{T_{z\theta}}{2R})\frac{\partial^2\delta\psi_\theta}{\partial\theta\partial x}-(\frac{T_{z\theta}}{2R^2})\frac{\partial^2\delta\psi_x}{\partial\theta^2}+(\frac{T_{xz}}{2})\frac{\partial^2\delta\psi_\theta}{\partial x^2}-\frac{Y_{xz}}{2R}\delta\psi_\theta\end{Bmatrix}Rdxd\theta \tag{7}$$

where classical and non-classical force and momentum are defined as below:

$$
\begin{aligned}
&(N_{xx}, N_{\theta\theta}, N_{x\theta}) = \int_{-h/2}^{h/2} (\sigma_{xx}, \sigma_{\theta\theta}, \sigma_{x\theta}) dz, \\
&(M_{xx}, M_{\theta\theta}, M_{x\theta}) = \int_{-h/2}^{h/2} (\sigma_{xx}, \sigma_{\theta\theta}, \sigma_{x\theta}) z dz, \\
&(Q_{xz}, Q_{z\theta}) = \int_{-h/2}^{h/2} k_s (\sigma_{xz}, \sigma_{z\theta}) dz, \\
&(Y_{xx}, Y_{\theta\theta}, Y_{zz}, Y_{x\theta}, Y_{xz}, Y_{z\theta}) = \int_{-h/2}^{h/2} (m_{xx}, m_{\theta\theta}, m_{zz}, m_{x\theta}, m_{xz}, m_{z\theta}) dz, \\
&(T_{xx}, T_{\theta\theta}, T_{zz}, T_{x\theta}, T_{xz}, T_{z\theta}) = \int_{-h/2}^{h/2} (m_{xx}, m_{\theta\theta}, m_{zz}, m_{x\theta}, m_{xz}, m_{z\theta}) z dz
\end{aligned}
\tag{8}
$$

Furthermore, the kinetic energy of the double walled cylindrical microshell can be expressed as:

$$
\delta T = \int_Z \iint_A \rho \left\{ \begin{array}{l} (\dfrac{\partial u}{\partial t} + z \dfrac{\partial \psi_x}{\partial t})(\dfrac{\partial}{\partial t}\delta u + z \dfrac{\partial}{\partial t}\delta \psi_x) \\ +(\dfrac{\partial v}{\partial t} + z \dfrac{\partial \psi_\theta}{\partial t})(\dfrac{\partial}{\partial t}\delta v + z \dfrac{\partial}{\partial t}\delta \psi_\theta) + (\dfrac{\partial w}{\partial t})\dfrac{\partial}{\partial t}\delta w \end{array} \right\} R\, dz\, dx\, d\theta \tag{9}
$$

The work done by Pasternak foundation, as the surrounding medium, acting on the double walled cylindrical microshell can be expressed as [30]:

$$
\delta W_3 = \left\{ K_w w + K_p \nabla^2 w \right\} \delta w \; R\, dV, \qquad \nabla^2 = \frac{\partial^2}{\partial x^2} + \frac{1}{R^2}\frac{\partial^2}{\partial \theta^2} \tag{10}
$$

In which K_w and K_p are the Winkler and Pasternak coefficients respectively. The energy dissipated by the dampers acting on the double walled cylindrical microshell by the surrounding medium can be expressed as [30]:

$$
\dot{\delta} D = \iiint_V \left\{ C_d \frac{\partial w}{\partial t}\frac{\partial}{\partial t}\dot{\delta} w \right\} R\, dV \tag{11}
$$

In which C_d is the damping constant. Now equations of motion and boundary conditions can be obtained substituting Eqs. (6), (9), (10), and (11) into (5), and integrating by parts.

For inner cylindrical microshell:

$$
\begin{aligned}
&\delta u_1 : \frac{\partial N^1_{xx}}{\partial x} + \frac{1}{R}\frac{\partial N^1_{x\theta}}{\partial \theta} + \frac{1}{2R^2}\left(-\frac{\partial Y^1_{\theta\theta}}{\partial \theta} + \frac{\partial Y^1_{zz}}{\partial \theta}\right) + \frac{1}{2R}\frac{\partial^2 Y^1_{zx}}{\partial \theta \partial x} + \frac{1}{2R^2}\frac{\partial^2 Y^1_{\theta z}}{\partial \theta^2} = I^1_0 \frac{\partial^2 u_1}{\partial t^2} + I^1_1 \frac{\partial^2 \psi_{1x}}{\partial t^2} \\
&\delta v_1 : \frac{\partial N^1_{x\theta}}{\partial x} + \frac{1}{R}\frac{\partial}{\partial \theta} N^1_{\theta\theta} + \frac{Q^1_{z\theta}}{R} + \frac{1}{2}\left\{ \begin{array}{l} \dfrac{1}{R}\dfrac{\partial}{\partial x}(-Y^1_{xx} + Y^1_{\theta\theta}) \\ -\dfrac{1}{R^2}\dfrac{\partial Y^1_{\theta x}}{\partial \theta} - \dfrac{\partial^2 Y^1_{xz}}{\partial x^2} - \dfrac{Y^1_{xz}}{R^2} - \dfrac{1}{R}\dfrac{\partial^2 Y^1_{z\theta}}{\partial \theta \partial x} \end{array} \right\} = I^1_0 \left[\frac{\partial^2 v_1}{\partial t^2} \right] + I^1_1 \left\{ \frac{\partial^2 \psi_{1\theta}}{\partial t^2} \right\} \\
&\delta w_1 : \frac{\partial Q^1_{xz}}{\partial x} + \frac{1}{R}\frac{\partial Q^1_{z\theta}}{\partial \theta} - \frac{N^1_{\theta\theta}}{R} - \frac{1}{2R^2}\frac{\partial^2 Y^1_{\theta x}}{\partial \theta^2} - \frac{1}{2R^2}\frac{\partial Y^1_{zx}}{\partial \theta} + \frac{1}{2R}\frac{\partial Y^1_{\theta z}}{\partial x} + \frac{\partial^2 Y^1_{x\theta}}{2\partial x^2} \\
&-\frac{1}{2R}\frac{\partial^2}{\partial \theta \partial x}(Y^1_{xx} - Y^1_{\theta\theta}) - \varsigma_1 v_x^2 \frac{\partial^2 w_1}{\partial x^2} - \varsigma_2 v_x \frac{\partial w_1}{\partial x} + \varsigma_3 v_x \frac{\partial^3 w_1}{\partial x^3} - K_1(w_1 - w_2) + \bar{F}\left(\frac{\partial^2 w}{\partial x^2} + \frac{\partial^2 v}{\partial x^2}\right) \\
&+K_{1p}\nabla^2(w_1 - w_2) - C_{1d}\left(\frac{\partial w_1}{\partial t} - \frac{\partial w_2}{\partial t}\right) = I^1_0\left(\frac{\partial^2 w_1}{\partial t^2}\right) + \varsigma_4 \frac{\partial^2 w_1}{\partial t^2} - \varsigma_5 v_x \frac{\partial^2 w_1}{\partial x\, \partial t} - \varsigma_6 \frac{\partial w_1}{\partial t} + \varsigma_7 \frac{\partial^3 w_1}{\partial t \partial x^2} \\
&\delta \psi_{1x} : \frac{\partial M^1_{xx}}{\partial x} + \frac{1}{R}\frac{\partial M^1_{\theta\theta}}{\partial \theta} - Q^1_{xz} + \frac{1}{2}\frac{\partial Y^1_{\theta x}}{\partial x} - \frac{1}{2R}\frac{\partial}{\partial \theta}(Y^1_{zz} - Y^1_{\theta\theta}) + \frac{Y^1_{zz}}{R} + \frac{1}{2R}\frac{\partial^2 T^1_{zx}}{\partial \theta \partial x} + \frac{1}{2R^2}\frac{\partial^2 T^1_{\theta z}}{\partial \theta^2} = I^1_1 \frac{\partial^2 u_1}{\partial t^2} + I^1_2 \frac{\partial^2 \psi_{1x}}{\partial t^2} \\
&\delta \psi_{1\theta} : \frac{1}{R}\frac{\partial M^1_{\theta\theta}}{\partial \theta} + \frac{\partial M^1_{x\theta}}{\partial x} - Q^1_{z\theta} + \frac{1}{2}\frac{\partial}{\partial x}\left(Y^1_{zz} - Y^1_{xx} + \frac{T^1_{\theta\theta}}{R}\right) - \frac{1}{2}\frac{\partial Y^1_{\theta x}}{\partial \theta} + \frac{Y^1_{xz}}{2R} - \frac{1}{2R}\frac{\partial^2 T^1_{\theta z}}{\partial \theta \partial x} - \frac{1}{2}\frac{\partial^2 T^1_{zx}}{\partial x^2} = I^1_1\left(\frac{\partial^2 v_1}{\partial t^2}\right) + I^1_2\left(\frac{\partial^2 \psi_{1\theta}}{\partial t^2}\right)
\end{aligned}
\tag{12}
$$

For outer cylindrical microshell:

$$\delta u_2 : \frac{\partial N^2_{xx}}{\partial x} + \frac{1}{R}\frac{\partial N^2_{x\theta}}{\partial \theta} + \frac{1}{2R^2}(-\frac{\partial Y^2_{\theta\theta}}{\partial \theta} + \frac{\partial Y^2_{zz}}{\partial \theta}) + \frac{1}{2R}\frac{\partial^2 Y^2_{zx}}{\partial \theta \partial x} + \frac{1}{2R^2}\frac{\partial^2 Y^2_{\theta z}}{\partial \theta^2} = I^2_0 \frac{\partial^2 u_2}{\partial t^2} + I^2_1 \frac{\partial^2 \psi_{2x}}{\partial t^2}$$

$$\delta v_2 : \frac{\partial N^2_{x\theta}}{\partial x} + \frac{1}{R}\frac{\partial}{\partial \theta}N^2_{\theta\theta} + \frac{Q^2_{z\theta}}{R} + \frac{1}{2}\left\{\begin{array}{l} \frac{1}{R}\frac{\partial}{\partial x}(-Y^2_{xx} + Y^2_{\theta\theta}) \\ -\frac{1}{R^2}\frac{\partial Y^2_{\theta x}}{\partial \theta} - \frac{\partial^2 Y^2_{xz}}{\partial x^2} - \frac{Y^2_{xz}}{R^2} - \frac{1}{R}\frac{\partial^2 Y^2_{z\theta}}{\partial \theta \partial x} \end{array}\right\} = I^2_0\left[\frac{\partial^2 v_2}{\partial t^2}\right] + I^2_1\left\{\frac{\partial^2 \psi_{2\theta}}{\partial t^2}\right\}$$

$$\delta w_2 : \frac{\partial Q^2_{xz}}{\partial x} + \frac{1}{R}\frac{\partial Q^2_{z\theta}}{\partial \theta} - \frac{N^2_{\theta\theta}}{R} - \frac{1}{2R^2}\frac{\partial^2 Y^2_{\theta x}}{\partial \theta^2} - \frac{1}{2R^2}\frac{\partial Y^2_{zx}}{\partial \theta} + \frac{1}{2R}\frac{\partial Y^2_{\theta z}}{\partial x} + \frac{\partial^2 Y^2_{x\theta}}{2\partial x^2} + \bar{F}(\frac{\partial^2 w}{\partial x^2} + \frac{\partial^2 v}{\partial x^2})$$
$$-\frac{1}{2R}\frac{\partial^2}{\partial \theta \partial x}(Y^2_{xx} - Y^2_{\theta\theta}) - K_1(w_2 - w_1) + K_{1p}\nabla^2(w_2 - w_1) - C_{1d}(\frac{\partial w_2}{\partial t} - \frac{\partial w_1}{\partial t}) - K_2(w_2) \quad (13)$$
$$+K_{2p}\nabla^2(w_2) - C_{2d}(\frac{\partial w_2}{\partial t}) = I^2_0(\frac{\partial^2 w_2}{\partial t^2})$$

$$\delta \psi_{2x} : \frac{\partial M^2_{xx}}{\partial x} + \frac{1}{R}\frac{\partial M^2_{\theta\theta}}{\partial \theta} - Q^2_{xz} + \frac{1}{2}\frac{\partial Y^2_{\theta x}}{\partial x} - \frac{1}{2R}\frac{\partial}{\partial \theta}(Y^2_{zz} - Y^2_{\theta\theta}) + \frac{Y^2_{zz}}{R} + \frac{1}{2R}\frac{\partial^2 T^2_{zx}}{\partial \theta \partial x} + \frac{1}{2R^2}\frac{\partial^2 T^2_{\theta z}}{\partial \theta^2} = I^2_1\frac{\partial^2 u_2}{\partial t^2} + I^2_2\frac{\partial^2 \psi_{2x}}{\partial t^2}$$

$$\delta \psi_{2\theta} : \frac{1}{R}\frac{\partial M^2_{\theta\theta}}{\partial \theta} + \frac{\partial M^2_{x\theta}}{\partial x} - Q^2_{z\theta} + \frac{1}{2}\frac{\partial}{\partial x}(Y^2_{zz} - Y^2_{xx} + \frac{T^2_{\theta\theta}}{R}) - \frac{1}{2}\frac{\partial Y^2_{\theta x}}{\partial \theta} + \frac{Y^2_{xz}}{2R} - \frac{1}{2R}\frac{\partial^2 T^2_{\theta z}}{\partial \theta \partial x} - \frac{1}{2}\frac{\partial^2 T^2_{zx}}{\partial x^2} = I^2_1\left(\frac{\partial^2 v_2}{\partial t^2}\right) + I^2_2\left(\frac{\partial^2 \psi_{2\theta}}{\partial t^2}\right)$$

Also, associate boundary conditions for each cylindrical microshell are as below:

$$\begin{aligned}
&\delta u = 0 \quad or \quad (N_{xx} + \frac{1}{4R}\frac{\partial Y_{xz}}{\partial \theta})n_x + (N_{x\theta} - \frac{Y_{\theta\theta} - Y_{zz}}{2R} + \frac{1}{4}\frac{\partial Y_{xz}}{\partial x} + \frac{1}{2R}\frac{\partial Y_{\theta z}}{\partial \theta})n_\theta = 0, \\
&\delta v = 0 \quad or \quad (N_{x\theta} + \frac{Y_{\theta\theta} - Y_{xx}}{2R} - \frac{1}{2}\frac{\partial Y_{xz}}{\partial x} - \frac{1}{4R}\frac{\partial Y_{\theta z}}{\partial \theta})n_x + (N_{\theta\theta} - \frac{1}{4R}\frac{\partial Y_{\theta z}}{\partial x} - \frac{Y_{\theta x}}{2R})n_\theta = 0, \\
&\delta w = 0 \quad or \quad (Q_{xz} + \frac{Y_{z\theta}}{2R} + \frac{1}{2}\frac{\partial Y_{x\theta}}{\partial x} + \frac{1}{4R}\frac{\partial (Y_{\theta\theta} - Y_{xx})}{\partial \theta})n_x + (Q_{\theta z} - \frac{Y_{zx}}{2R} - \frac{1}{2R}\frac{\partial Y_{x\theta}}{\partial \theta} + \frac{1}{4}\frac{\partial (Y_{\theta\theta} - Y_{xx})}{\partial x})n_\theta = 0, \\
&\delta \psi_x = 0 \quad or \quad (M_{xx} + \frac{1}{4R}\frac{\partial T_{xz}}{\partial \theta} + \frac{Y_{x\theta}}{2})n_x + (M_{\theta x} + \frac{1}{4}\frac{\partial T_{xz}}{\partial x} + \frac{1}{2R}\frac{\partial T_{\theta z}}{\partial \theta} + \frac{(Y_{\theta\theta} - Y_{zz})}{2})n_\theta = 0, \\
&\delta \psi_\theta = 0 \quad or \quad (M_{x\theta} - \frac{(Y_{xx} - Y_{zz})}{2} - \frac{1}{4R}\frac{\partial T_{\theta z}}{\partial \theta} - \frac{1}{2}\frac{\partial T_{xz}}{\partial x} + \frac{T_{\theta\theta}}{2R})n_x + (M_{\theta\theta} - \frac{Y_{x\theta}}{2} - \frac{1}{4}\frac{\partial T_{\theta z}}{\partial x})n_\theta = 0,
\end{aligned} \quad (14)$$

For example:
The clamped boundary conditions at x=0, L:

$$u = v = w = \psi_x = \psi_\theta = 0 \quad (15)$$

The simply supported boundary conditions at x=0, L:

$$v = w = \psi_\theta = 0, \qquad (N_{xx} + \frac{1}{4R}\frac{\partial Y_{xz}}{\partial \theta}) = 0, \qquad (M_{xx} + \frac{1}{4R}\frac{\partial T_{xz}}{\partial \theta} + \frac{Y_{x\theta}}{2}) = 0. \quad (16)$$

3 SOLUTION PROCEDURE

Generalized Differential Quadrature method (GDQ) has comprehensively used to solve the governing equations of motion in these structure [32-34]. Surveying the literature reveals the shortcoming of investigations in order to the analysis of the moderately thick cylindrical nano-shell considering the modified couple stress and centrifugal force. In this study, GDQ method is used to calculate the spatial derivatives of field variables in equilibrium equations. In

the implementation of GDQ, Grid points describe the locations of calculated derivatives and field variables. Thus, the *"r – th"* order derivative of a function *"f(x)"* can be defined as the linear sum of the function values which is: [35]

$$\left.\frac{\partial^r f\left(x\right)}{\partial x^{\,r}}\right|_{x=x_P}=\sum_{j=1}^{n}C_{ij}^{(r)}f\left(x_i\right) \tag{17}$$

where, *n* is the number of grid points along the *x* direction. Also, C_{ij} is obtained as follows:

$$C_{ij}^{(1)}=\begin{cases}\dfrac{M\left(r_i\right)}{\left(r_i-r_j\right)M\left(r_j\right)} & i\neq j\\ -\sum\limits_{j=1,i\neq j}^{n}C_{ij}^{(1)} & i=j\end{cases} \tag{18}$$

and *M* is defined as:

$$M\left(x_i\right)=\prod_{j=1,j\neq i}^{n}\left(x_i-x_j\right) \tag{19}$$

Superscript *"r"* is the order of the derivative. Also, $C^{(r)}$ is the weighing coefficient along the *x* direction, which could be written as:

$$C_{ij}^{(r)}=\begin{cases}r\left[C_{ij}^{(r-1)}C_{ij}^{(1)}-\dfrac{C_{ij}^{(r-1)}}{\left(r_i-r_j\right)}\right] & i\neq j\ and\ 2\le r\le n-1\\ -\sum\limits_{j=1,i\neq j}^{n}C_{ij}^{(r)} & i=j\ and\ 1\le r\le n-1\end{cases} \tag{20}$$

In order to obtain a better mesh point distribution, Chebyshev-Gauss-Lobatto technique has been defined:

$$r_i=\frac{1}{2}\left(1-\cos\left(\frac{\left(i-1\right)}{\left(N-1\right)}\pi\right)\right)\qquad i=1,2,3,\ldots,n \tag{21}$$

Applying Eq. (21) into the governing and B.C equations, for each cylindrical microshell have:

$$\left\{\begin{bmatrix}[M_{dd}] & [M_{db}]\\ [M_{bd}] & [M_{bb}]\end{bmatrix}\omega^2+\begin{bmatrix}[C_{dd}] & [C_{db}]\\ [C_{bd}] & [C_{bb}]\end{bmatrix}\omega+\begin{bmatrix}[K_{dd}] & [K_{db}]\\ [K_{bd}] & [K_{bb}]\end{bmatrix}\right\}\begin{Bmatrix}\delta_d\\ \delta_b\end{Bmatrix}=0 \tag{22}$$

In which the subscripts *b* and *d* refer to the boundary and domain grid points, respectively. Also δ define the displacement vector. Eq. (22) can be transformed to a standard eigenvalue problem:

$$\begin{aligned}&[K^*]\{\delta_i\}=\left(\omega^2\right)[M^*]\{\delta_i\}+\left(\omega\right)[C^*]\{\delta_i\}\\ &[K^*]=[K_{dd}-K_{db}K_{bb}^{\ -1}K_{bd}]\\ &[C^*]=[C_{dd}-C_{db}K_{bb}^{\ -1}K_{bd}]\\ &[M^*]=[M_{dd}-M_{db}K_{bb}^{\ -1}K_{bd}]\end{aligned} \tag{23}$$

Finally, with setting this polynomial to zero, we can find natural frequency of the microstructure.

4 RESULTS

The numerical results of the vibration behavior of double walled cylindrical FG microshell are investigated based on the MCST for the various boundary conditions. Sufficient number of grid points is necessary to achieve accurate results in GDQ method. As it is shown in Table 1., for the good results, 31 grid points are appropriate. The Results are shown and analyzed in two sections. The first one verifies proposed model with existing literatures. Second section shows the effect of length, thickness, FG power index, Winkler and Pasternak coefficient and shear correction factor on the natural frequency of double walled cylindrical FG microshell.

Table 1
The effect of the number of grid points on evaluating convergence of the natural frequency of the double FG cylindrical microshell with respect to the different FG power index, boundary conditions with $L_1 = L_2 = 10\mu m$, $L_1 / R_1 = 10$, $h_1 = h_2 = R_1 / 10$, $l_{1m} = 14\mu m$, $l_{1c} = l_{1m} / 2$, $l_{1m} = l_{2m}$, $l_{1c} = l_{2c}$, $K_w = 1e14$, $K_p = 0$ and $R_2 = 1.125 \times R_1$.

B.Cs	FG power index (m)	N=15	N=19	N=23	N=27	N=31	N=34
Simply-Simply	Only metal	0.48146166	0.48146166	0.48146166	0.48146166	0.48146166	0.48146166
	1	0.68933699	0.68933699	0.68933699	0.68933699	0.68933699	0.68933699
	10	0.80166448	0.80166448	0.80166448	0.80166448	0.80166448	0.80166448
	Only ceramic	0.82412107	0.82412107	0.82412107	0.82412107	0.82412107	0.82412107
Clamp-Simply	Only metal	0.56806511	0.56794809	0.56794649	0.56794853	0.56794852	0.56794852
	1	0.87162888	0.87146831	0.87144774	0.87145249	0.87145264	0.87145264
	10	1.03504190	1.03490931	1.03489181	1.03489577	1.03489582	1.03489582
	Only ceramic	1.06745638	1.06732910	1.06731387	1.06731751	1.06731752	1.06731752
Clamp-Clamp	Only metal	0.66162622	0.66164744	0.66164278	0.66164272	0.66164274	0.66164274
	1	1.06307791	1.06314833	1.06313858	1.06313795	1.06313800	1.06313800
	10	1.27890989	1.27897364	1.27896266	1.27896217	1.27896221	1.27896221
	Only ceramic	1.32155387	1.32161012	1.32159908	1.32159869	1.32159873	1.32159873

4.1 Model validation

For results verification of this work with other articles, Table 2 and Fig. 2 give a comparison of results for dimensionless natural frequency, of the simply supported cylindrical nanoshell between the presented results with those obtained by other articles, for different geometrical parameters. Table 2 shows the obtained results for dimensionless natural frequency of simply supported cylindrical nanoshell for difference length scale parameter. They are in good agreement with those given by Ref [36]. Another verification of this work, according to Fig. 2, it is revealed that the proposed modeling can provide good agreement with molecular dynamic simulation. In this Figure show that, as $l = R/3$, the results of the current research based on FSDT are very similar to those of MD simulation. In addition, this issue is reported by Refs [37, 38] .The material properties of single-walled carbon nanotubes are presented in Table 3.

Table 2
Comparison of dimensionless first three natural frequencies of isotropic homogeneous nanoshells, with different thicknesses.

h/R	n	Ref [36] (l=0)	Present (l=0)	Ref [36] (l=h)	Present study (l=h)
0.02	1	0.1954	0.19536215	0.1955	0.19543206
	2	0.2532	0.25271274	0.2575	0.25731258
	3	0.2772	0.27580092	0.3067	0.30621690
0.05	1	0.1959	0.19542305	0.1963	0.19585782
	2	0.2623	0.25884786	0.2869	0.28543902
	3	0.3220	0.31407326	0.4586	0.45457555

Table 3
The material properties of single-walled carbon nanotubes.

E	v	h	ρ
1.06 *TPa*	0.19	0.34 *nm*	2300 kg/m^3

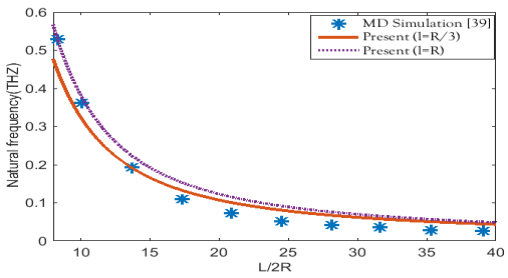

Fig.2
Comparison of the natural frequency of cylindrical nanoshell with the results obtained by MD simulation [39].

4.2 Parametric results

The material for this paper is FG for inner and outer layer of the cylindrical microshell and it is assumed that the inner surface is ceramic and the outer one is metal. Volume fraction index (m) determines the variation profile of the material properties across the thickness of the FG cylindrical microshell. The material properties are given in Table 4.

Table 4
Material properties of FGM constituents.

Material properties	Unit	Aluninum	Silicon
E	GPA	70	210
ρ	Kg/m^3	2700	2370
v	-	0.3	0.24

Table 4 gives a presentation of shear correction factor, thickness, winkler and pasternak stiffness effect on natural frequency under the various boundary conditions. As it can be seen from Table 5, an increase in shear correction factor leads to an increase in the natural frequency. This trend is observed under all types of boundary conditions. In addition, the increase in the winkler and Pasternak stiffness of the frequency results in considerable increase in natural frequency. Simply-Simply boundary condition has the lowest frequency because of its particular condition, and Clamp-Clamp boundary condition has the highest frequency. In addition, the effect of Pasternak stiffness (K_p) has the high effect on the natural frequency in compare with winkler stiffness Also, by increasing the thickness, the natural frequency tends to decrease.

Table5
Variation of the fundamental natural frequency, with different thickness of a double walled FG cylindrical microshell for different shear correction factor, winker and pasternak stiffness with various boundary conditions and $L_1 = L_2 = 10\mu m$, $L_1 / R_1 = 10$, $h_1 = h_2$, $l_{1m} = 14\mu m$, $l_{1c} = l_{1m} / 2$, $l_{1m} = l_{2m}$, $l_{1c} = l_{2c}$, $R_2 = 1.125 \times R_1$, $m = 1$.

B.Cs	K_p =0				K_p =100			
	K_s =0		K_s =5/6		K_s =0		K_s =5/6	
Simply_Simply	K_w =1e14	K_w =1e15	K_w =1e14	K_w =1e15	K_w =1e14	K_w =1e15	K_w =1e14	K_w =1e15
$h_1(\mu m)$								
0.1	0.687427	1.19883	0.689337	1.20122	0.778507	1.24393	0.780368	1.24645
0.2	0.636747	0.961331	0.641959	0.965259	0.692019	0.990906	0.696887	0.994775
0.3	0.617666	0.863184	0.628401	0.871239	0.657995	0.886043	0.668113	0.893923
Simply_Clamp								
$h_1(\mu m)$								
0.1	0.866874	1.331686	0.8716289	1.336483	0.9472032	1.374034	1.378875	0.9517374
0.2	0.8242185	1.112314	0.8339751	1.120407	0.8710811	1.139584	1.147561	0.8803839
0.3	0.8086962	1.022929	0.8254644	1.036825	0.8420691	1.043792	1.057477	0.858198
Clamp_Clamp								
$h_1(\mu m)$								
0.1	1.055548	1.484719	1.063078	1.492008	1.12715	1.524666	1.134418	1.531971
0.2	1.018709	1.279139	1.034333	1.292736	1.059203	1.30451	1.074339	1.317973
0.3	1.005598	1.196397	1.031063	1.218672	1.03397	1.215613	1.058798	1.237657

Figs. 3-5 show the effect of the length on natural frequency (*GHz*) of double walled cylindrical FG microshell with different boundary conditions and $R_1 = 1\mu m$, $h_1 = h_2 = R_1/10$, $l_{1m} = 14\mu m$, $l_{1c} = l_{1m}/2$, $l_{1m} = l_{2m}$, $l_{1c} = l_{2c}$, $K_w = 1e14$, $K_p = 100$, $R_2 = 1.125 \times R_1$. It can be seen from Figs. 3-5 that the increase in length leads to the increase in natural frequency. This is because increasing the length is eventuated to decrease in stiffness and natural frequency of the double FG cylindrical microshell. Other results are that, the double cylindrical microshell which, is made of only metal, has the lower frequency compare with only ceramic. The other remarkable point is related to Fig.3 where the effect of length on natural frequency of simply-simply boundary condition is less than two others.

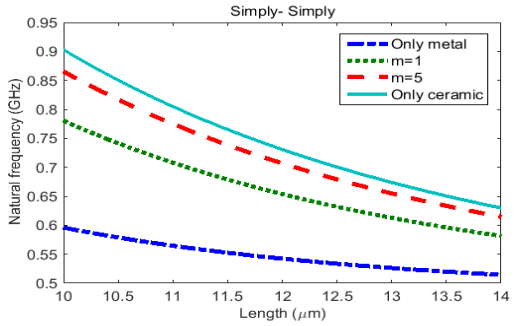

Fig.3
The effect of length on the natural frequency with simply-simply boundary conditions.

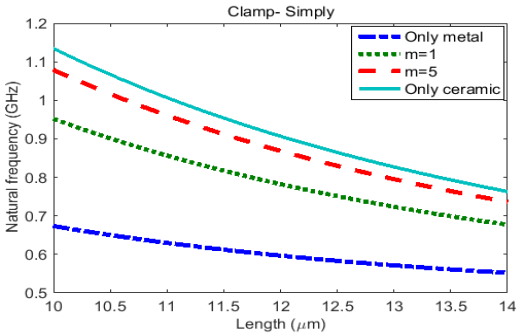

Fig.4
The effect of length on the natural frequency with clamp-simply boundary conditions.

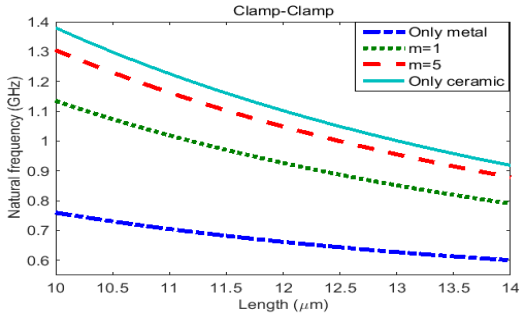

Fig.5
The effect of length on the natural frequency with clamp-clamp boundary conditions.

Figs. 6-8 illustrate the effect of Winkler foundation on natural frequency of double walled cylindrical microshell for the case where $L_1 = L_2 = 10\mu m$, $L_1/R_1 = 10$, $h_1 = h_2 = R_1/10$, $l_{1m} = 14\mu m$, $l_{1c} = l_{1m}/2$, $l_{1m} = l_{2m}$, $l_{1c} = l_{2c}$, $K_p = 100$, $R_2 = 1.125 \times R_1$. Figs. 6-8 respectively are related to the simply-simply, clamped-simply and clamp-clamp boundary conditions. As we can see in all three figures, with increase in Winkler stiffness, natural frequencies increase. Also increase in FG power index leads to increase in natural frequencies. In simply-simply, frequency variations are modest again. Figs. 6-8 show that with considering the coefficient of Pasternak, there is an exceptional trend by increasing Winkler coefficient, at first frequency increase and reach to a peak point then the natural frequency tends to be constant in all boundary conditions.

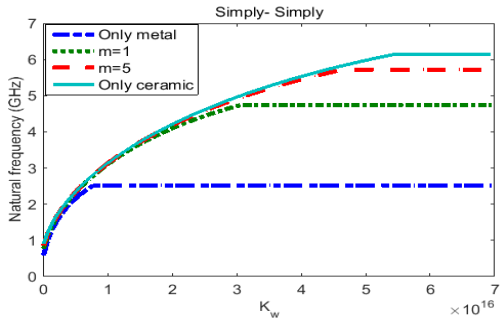

Fig.6
The effect of Winkler stiffness on the natural frequency with simply-simply boundary conditions.

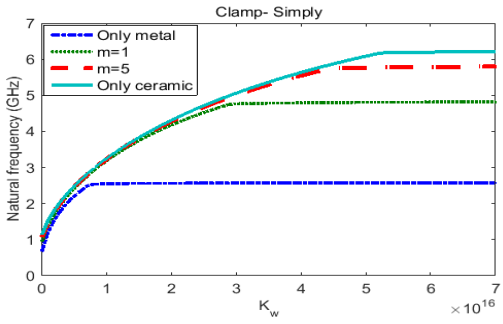

Fig.7
The effect of Winkler stiffness on the natural frequency with clamp-simply boundary conditions.

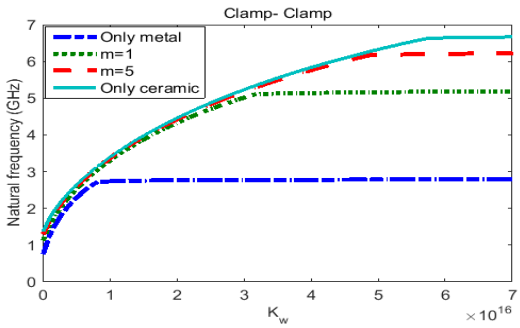

Fig.8
The effect of Winkler stiffness on the natural frequency with clamp-clamp boundary conditions.

Figs. 9-11 illustrate the effect of Pasternak foundation on natural frequency with $L_1 = L_2 = 10\mu m$, $L_1 / R_1 = 10$, $h_1 = h_2 = R_1 / 10$, $l_{1m} = 14\mu m$, $l_{1c} = l_{1m} / 2$, $l_{1m} = l_{2m}$, $l_{1c} = l_{2c}$, $K_w = 1e14$, $R_2 = 1.125 \times R_1$. Figs. 9-11 respectively are related to simply-simply, clamped-simply and clamp-clamp boundary conditions; as it is obvious in all figures with increase in Pasternak stiffness the natural frequencies tend to increase. Also increase in FG power index causes to increase in natural frequencies. Also, this kind of foundation has more influence on frequency in comparison with Winkler. In simply-simply, frequency variations are modest again. Figs. 9-11 show that with considering the coefficient of Winkler, there is an exceptional trend by increasing Pasternak coefficient, at first frequency increase and reach to a peak point then the natural frequency tends to be constant in all boundary conditions.

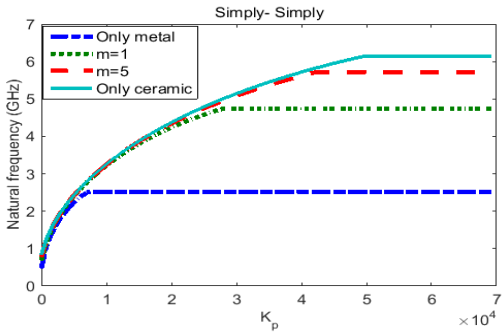

Fig.9
The effect of Pasternak stiffness on the natural frequency with simply-simply boundary conditions.

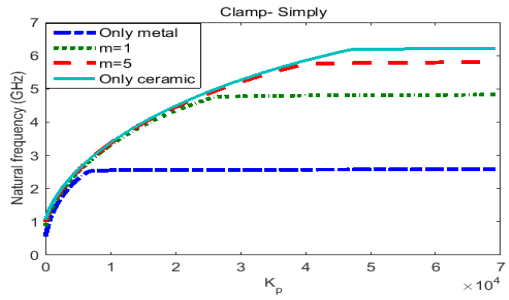

Fig.10
The effect of Pasternak stiffness on the natural frequency with clamp-simply boundary conditions.

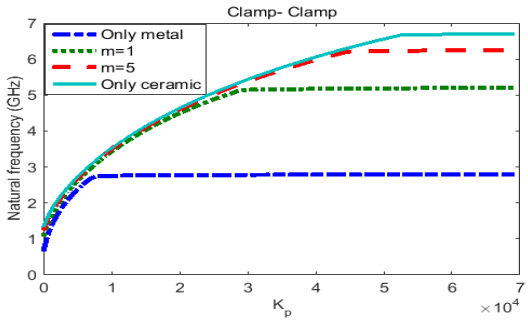

Fig.11
The effect of Pasternak stiffness on the natural frequency with clamp-clamp boundary conditions.

Figs. 12-14 demonstrates the effect of dampers on the natural frequency of the double walled cylindrical microshell with $L_1 = L_2 = 10\mu m$, $L_1 / R_1 = 10$, $h_1 = h_2 = R_1 / 10$, $l_{1m} = 14\mu m$, $l_{1c} = l_{1m} / 2$, $l_{1m} = l_{2m}$, $l_{1c} = l_{2c}$, $K_w = 1e14$ and $R_2 = 1.125 \times R_1$. In addition, Figs. 9-11 respectively are related to simply-simply, clamped-simply and clamp-clamp boundary conditions. It can be understood from Fig. 12 that increase in the dampers constant reduces the natural frequency of the microstructure, but the reduction of the frequency is more intense in the greater constants of FG power index (only ceramic). The difference between Figs. 12, 13 and 14 is that, while a B.Cs changes from simply-simply to clamp- clamp, the natural frequency increases. This is because, clamp- clamp B.Cs improves the structure stability.

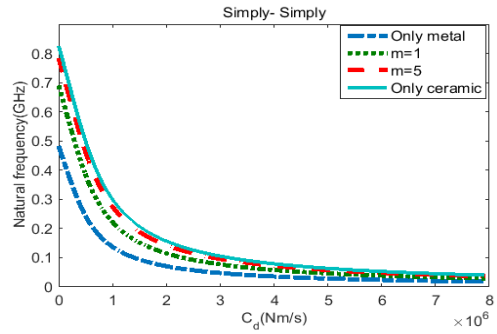

Fig.12
The effect of damping stiffness on the natural frequency with simply-simply boundary conditions.

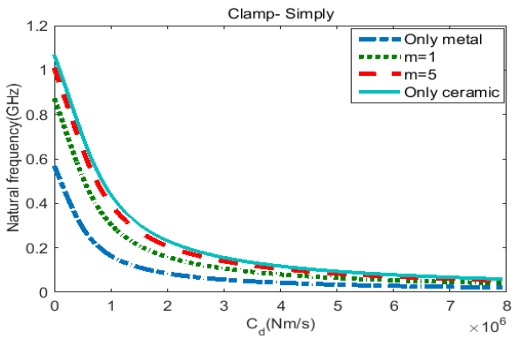

Fig.13
The effect of damping stiffness on the natural frequency with clamp-simply boundary conditions.

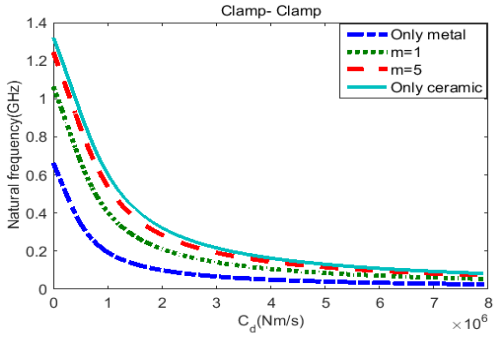

Fig.14
The effect of damping stiffness on the natural frequency with clamp-clamp boundary conditions.

5 CONCLUSIONS

This paper presents the free vibration analysis of double walled FG cylindrical microshell surrounded by viscoelastic foundation. MCST introduces the size-dependent effect. The equations of motion and non-classic boundary conditions is derived using Hamilton's principle. In addition, for confirmation, the result of current model is validated with the results obtained from molecular dynamics (MD) simulation. Considering length scale parameter (l=R/3) on MCST show, the results have better agreement with MD simulation. The natural frequency of the double walled cylindrical FG microshell is investigated with respect to the length, thickness, FG power index, damping constant, Winkler-Pasternak coefficients and shear correction factor for different boundary conditions of the double cylindrical FG microshell. The followings important results can be obtained from this study:

1- By increasing the damping constant, length and thickness the natural frequency tend to decrease while, by increasing the FG power index, the natural frequency increases.
2- Simply-simply boundary condition has the lowest natural frequency because of its particular condition, and Clamp-Clamp boundary condition has the highest natural frequency.
3- The results show that, increase in the length to radius ratio and material length scale parameter lead to increase in the critical speed of the rotation FG cylindrical nanoshell.
4- By considering the coefficient of Winkler and Pasternak, there is an exceptional trend by increasing Winkler and Pasternak coefficient, at first frequency increase and reach to a peak point then the natural frequency tends to be constant in all boundary conditions.

REFERENCES

[1] Reddy J., Chin C., 1998, Thermomechanical analysis of functionally graded cylinders and plates, *Journal of Thermal Stresses* **21**: 593-626.
[2] Loy C., Lam K., Reddy J., 1999, Vibration of functionally graded cylindrical shells, *International Journal of Mechanical Sciences* **41**: 309-324.
[3] Pradhan S., Loy C., Lam K., Reddy J., 2000, Vibration characteristics of functionally graded cylindrical shells under various boundary conditions, *Applied Acoustics* **61**: 111-129.
[4] Patel B., Gupta S., Loknath M., Kadu C., 2005,Free vibration analysis of functionally graded elliptical cylindrical shells using higher-order theory, *Composite Structures* **69**: 259-270.
[5] Kadoli R., Ganesan N., 2006, Buckling and free vibration analysis of functionally graded cylindrical shells subjected to a temperature-specified boundary condition, *Journal of Sound and Vibration* **289**: 450-480.
[6] Zhi-Yuan C., Hua-Ning W., 2007, Free vibration of FGM cylindrical shells with holes under various boundary conditions, *Journal of Sound and Vibration* **306**: 227-237.
[7] Haddadpour H., Mahmoudkhani S., Navazi H., 2007, Free vibration analysis of functionally graded cylindrical shells including thermal effects, *Thin-walled Structures* **45**: 591-599.
[8] Farid M., Zahedinejad P., Malekzadeh P., 2010,Three-dimensional temperature dependent free vibration analysis of functionally graded material curved panels resting on two-parameter elastic foundation using a hybrid semi-analytic, differential quadrature method, *Materials & Design* **31**: 2-13.
[9] Rahaeifard M., Kahrobaiyan M., Ahmadian M., 2009, Sensitivity analysis of atomic force microscope cantilever made of functionally graded materials, *International Design Engineering Technical Conferences and Computers and Information in Engineering Conference*.

[10] Fu Y., Du H., Huang W., Zhang S., Hu M., 2004, TiNi-based thin films in MEMS applications: a review, *Sensors and Actuators A: Physical* **112**: 395-408.
[11] Witvrouw A., Mehta A., 2005, The use of functionally graded poly-SiGe layers for MEMS applications, *Materials Science Forum* **2005**: 255-260.
[12] Lee Z., Ophus C., Fischer L., Nelson-Fitzpatrick N., Westra K., Evoy S., 2006, Metallic NEMS components fabricated from nanocomposite Al–Mo films, *Nanotechnology* **17**: 3063.
[13] Shojaeian M., Beni Y.T., 2015, Size-dependent electromechanical buckling of functionally graded electrostatic nano-bridges, *Sensors and Actuators A: Physical* **232**: 49-62.
[14] Mescher M. J., Houston K., Bernstein J. J., Kirkos G. A., Cheng J., Cross L. E., 2002, Novel MEMS microshell transducer arrays for high-resolution underwater acoustic imaging applications, *Proceedings of IEEE*.
[15] Toupin R. A., 1962, Elastic materials with couple-stresses, *Archive for Rational Mechanics and Analysis* **11**: 385-414.
[16] Koiter W., 1964, Couple stresses in the theory of elasticity, *Proceedings van de Koninklijke Nederlandse Akademie van Wetenschappen.*
[17] Mindlin R. D., 1964, Micro-structure in linear elasticity, *Archive for Rational Mechanics and Analysis* **16**: 51-78.
[18] Asghari M., Kahrobaiyan M., Rahaeifard M., Ahmadian M., 2011, Investigation of the size effects in Timoshenko beams based on the couple stress theory, *Archive of Applied Mechanics* **81**: 863-874.
[19] Park S., Gao X., 2006, Bernoulli–Euler beam model based on a modified couple stress theory, *Journal of Micromechanics and Microengineering* **16**: 2355.
[20] Reddy J., 2011, Microstructure-dependent couple stress theories of functionally graded beams, *Journal of the Mechanics and Physics of Solids* **59**: 2382-2399.
[21] Shaat M., Mahmoud F., Gao X.-L., Faheem A. F., 2014, Size-dependent bending analysis of Kirchhoff nano-plates based on a modified couple-stress theory including surface effects, *International Journal of Mechanical Sciences* **79**: 31-37.
[22] Miandoab E. M., Pishkenari H. N., Yousefi-Koma A., Hoorzad H., 2014, Polysilicon nano-beam model based on modified couple stress and Eringen's nonlocal elasticity theories, *Physica E: Low-dimensional Systems and Nanostructures* **63**: 223-228.
[23] Karami H., Farid M., 2015, A new formulation to study in-plane vibration of curved carbon nanotubes conveying viscous fluid, *Journal of Vibration and Control* **21**: 2360-2371.
[24] Choi J., Song O., Kim S.-k., 2013, Nonlinear stability characteristics of carbon nanotubes conveying fluids, *Acta Mechanica* **224**: 1383-1396.
[25] Zhang Y.-W., Yang T.-Z., Zang J., Fang B., 2013, Terahertz wave propagation in a nanotube conveying fluid taking into account surface effect, *Materials* **6**: 2393-2399.
[26] Chang T.-P., 2013, Axial vibration of non-uniform and non-homogeneous nanorods based on nonlocal elasticity theory, *Applied Mathematics and Computation* **219**: 4933-4941.
[27] Ali-Asgari M., Mirdamadi H. R., Ghayour M., 2013, Coupled effects of nano-size, stretching, and slip boundary conditions on nonlinear vibrations of nano-tube conveying fluid by the homotopy analysis method, *Physica E: Low-dimensional Systems and Nanostructures* **52**: 77-85.
[28] Kiani K., 2013, Vibration behavior of simply supported inclined single-walled carbon nanotubes conveying viscous fluids flow using nonlocal Rayleigh beam model, *Applied Mathematical Modelling* **37**: 1836-1850.
[29] Arani A. G., Ahmadi M., Ahmadi A., Rastgoo A., Sepyani H., 2012, Buckling analysis of a cylindrical shell, under neutron radiation environment, *Nuclear Engineering and Design* **242**: 1-6.
[30] Ghorbanpour A., Mosallaie A. A., Kolahchi R., 2014, Nonlinear dynamic buckling of viscous-fluid-conveying PNC cylindrical shells with core resting on visco-pasternak medium **6**(3): 265-277.
[31] Wattanasakulpong N., Ungbhakorn V., 2014, Linear and nonlinear vibration analysis of elastically restrained ends FGM beams with porosities, *Aerospace Science and Technology* **32**: 111-120.
[32] Ghadiri M., Shafiei N., 2015, Nonlinear bending vibration of a rotating nanobeam based on nonlocal Eringen's theory using differential quadrature method, *Microsystem Technologies* **22**: 2853-2867.
[33] Daneshjou K., Talebitooti M., Talebitooti R., Googarchin H. S., 2013, Dynamic analysis and critical speed of rotating laminated conical shells with orthogonal stiffeners using generalized differential quadrature method, *Latin American Journal of Solids and Structures* **10**: 349-390.
[34] Daneshjou K., Talebitooti M., Talebitooti R., 2013, Free vibration and critical speed of moderately thick rotating laminated composite conical shell using generalized differential quadrature method, *Applied Mathematics and Mechanics* **34**: 437-456.
[35] Shu C., 2012, *Differential Quadrature and its Application in Engineering*, Springer Science & Business Media.
[36] Tadi Beni Y., Mehralian F., Zeighampour H., 2016, The modified couple stress functionally graded cylindrical thin shell formulation, *Mechanics of Advanced Materials and Structures* **23**: 791-801.
[37] Ghadiri M., Safarpour H., 2016, Free vibration analysis of embedded magneto-electro-thermo-elastic cylindrical nanoshell based on the modified couple stress theory, *Applied Physics A* **122**: 833.
[38] Barooti M. M., Safarpour H., M., 2017, Critical speed and free vibration analysis of spinning 3D single-walled carbon nanotubes resting on elastic foundations, *The European Physical Journal Plus* **132**: 6.
[39] Ansari R., Gholami R., Rouhi H., 2012, Vibration analysis of single-walled carbon nanotubes using different gradient elasticity theories, *Composites Part B: Engineering* **43**: 2985-2989.